Phosphine Complexes of Yttrium, Lanthanum, and Lutetium. Synthesis, Thermolysis, and Fluxional Behavior of the Hydrocarbyl Derivatives $MR'[N(SiMe_2CH_2PMe_2)_2]_2$. X-ray Crystal Structure of $\overline{Y[N(SiMe_2CHPMe_2)(SiMe_2CH_2PMe_2)]}[N(SiMe_2CH_2PMe_2)_2]$

Michael D. Fryzuk,*,† T. S. Haddad, and Steven J. Rettig‡

Department of Chemistry, University of British Columbia, 2036 Main Mall, Vancouver, BC, Canada V6T 1Z1

Received January 22, 1991

The preparation of phosphine complexes of the group 3 elements yttrium and lanthanum and the lanthanide metal lutetium is described. The reaction of 2 equiv of lithium salt of the mixed-donor ligand $LiN(SiMe_2CH_2PR_2)_2$ (R = Me, Ph, Pr^i) with YCl_3 or $LuCl_3$ (R = Me only) leads to the formation of the bis(ligand) complexes $MCl[N(SiMe_2CH_2PR_2)_2]_2$. The analogous lanthanum derivative requires the use of the corresponding potassium salt $KN(SiMe_2CH_2PR_2)_2$ (R = Me, Ph) with anhydrous $LaCl_3$ to generate good yields of $LaCl[N(SiMe_2CH_2PR_2)_2]_2$. Replacement of the remaining chloride with a hydrocarbyl ligand can be achieved for M = Y and Lu to generate $MR[N(SiMe_2CH_2PMe_2)_2]_2$ (M = Y, R = Ph, CH_2Ph; M = Lu, R = Ph). These hydrocarbyl complexes are thermally unstable and undergo a cyclometalation reaction to generate complexes having the formula $\overline{M[N(SiMe_2CHPMe_2)(SiMe_2CH_2PMe_2)]}[N(SiMe_2CH_2PMe_2)_2]$; the analogous lanthanum complex is formed directly upon attempted metathesis of the corresponding chloride with PhLi. All of these seven-coordinate metal phosphine complexes are fluxional, apparently exchanging sites via phosphine arm dissociation and rearrangement. The kinetics of the cyclometalation reaction were carried out and found to have $\Delta H^\ddagger = 20.5$ (1) kcal/mol and $\Delta S^\ddagger = -3$ (3) eu; the relatively small but negative $\Delta S^\ddagger$ is attributed to a four-membered transition state having a dissociated phosphine. In addition, an inverse isotope effect of $k_H/k_D = 0.85$–0.92 (temperature dependent) was observed for the cyclometalation of $Y(CH_2Ph)[N(SiMe_2CH_2PR_2)_2]_2$ vs $Y(CD_2C_6D_5)[N(SiMe_2CH_2PR_2)_2]_2$; a preequilibrium involving an agostic η^2-benzyl going η^1 is consistent with this observation. Crystals of $\overline{Y[N(SiMe_2CHPMe_2)(SiMe_2CH_2PMe_2)]}[N(SiMe_2CH_2PMe_2)_2]$ are monoclinic, $a = 18.115$ (1) Å, $b = 15.875$ (8) Å, $c = 12.706$ (2) Å, $\beta = 92.619$ (7)°, $Z = 4$, $\rho_c = 1.181$ g cm^{-3}, and space group $P2_1/c$. The structure was solved by the Patterson method and was refined by full-matrix least-squares procedures to $R = 0.063$ and $R_w = 0.073$ for 3270 reflections with $I \geq 3\sigma(I)$. Attempts to use the cyclometalated derivative in σ-bond metathesis reactions were only successful with D_2; no reaction was observed with hydrocarbons.

Introduction

The phosphine ligand has played a pivotal role in the development of modern inorganic chemistry.[1] Not only has this donor type been useful in fundamental studies of reaction mechanisms but also many industrial processes for the production of useful synthetic materials utilize phosphine-based metal catalysts.[2] In fact, given the ability to tailor steric and electronic effects in phosphorus ligands by the varying the substituents and the fact that the phosphorus-31 nucleus provides a superb NMR handle on structure and reactivity, it is not surprising that this donor type is the premiere ligand for most of the metals throughout the periodic table.

However, there are some elements for which neutral, phosphorus-based ligands are still rare or even unknown.[3] In particular, phosphine complexes of the group 3 metals and the lanthanide elements are extremely sparse, with only a few genuine derivatives having been reported.[4-7] The paucity of such compounds has been ascribed to the *hard* acid nature of these metals and the *soft* base nature of the phosphine donor, which results in a mismatch of donor and acceptor. However, while there might not be a preference for phosphine donors to bind to these elements, given no other choice, phosphine complexes should be attainable. It would appear to be a matter of selecting the appropriate solvent (i.e., avoiding ethers) and ensuring that hard ligands are not present in excess.

Our strategy for overcoming this apparent mismatch of donor and acceptor is to use the hybrid chelating ligand $[N(SiMe_2CH_2PR_2)_2]^-$ (I; R = Me, Pr^i, Ph). It was anticipated that the hard amide donor NR_2^- would serve as an anchor to the metal, thereby inducing chelation of the pendant phosphine donors by virtue of their close proximity to the metal. For the group 4 elements, this strategy holds, as we have been able to generate a variety of phosphine-stabilized complexes.[8] In this paper we extend this concept to the group 3 elements yttrium and lantha-

† E. W. R. Steacie Fellow (1990–92).
‡ Experimental officer: UBC Crystallographic Service.

(1) McAuliffe, C. A. In *Comprehensive Coordination Chemistry*; Wilkinson, G., Gillard, R. D., McCleverty, J. A., Eds.; Pergammon: London, 1987; Vol. 2, p 989.
(2) Pignolet, L. H., Ed. *Homogeneous Catalysis with Metal Phosphine Complexes*; Plenum: New York, 1983.
(3) For a recent review see: Fryzuk, M. D.; Haddad, T. S.; Berg, D. J. *Coord. Chem. Rev.* **1990**, *99*, 137.
(4) Fryzuk, M. D.; Haddad, T. S. *J. Am. Chem. Soc.* **1988**, *110*, 8263.
(5) Group 3 phosphine complexes: (a) Hitchcock, P. B.; Lappert, M. F.; MacKinnon, I. A. *J. Chem. Soc., Chem. Commun.* **1988**, 1557. (b) Piers, W. E.; Shapiro, P. J.; Bunel, E. E.; Bercaw, J. E. *Synlett.* **1990**, *1*, 74.
(6) Lanthanide phosphine complexes: (a) Stults, S.; Zalkin, A. *Acta Crystallogr.* **1987**, *C43*, 430. (b) Brennan, J. G.; Stults, S. D.; Andersen, R. A.; Zalkin, A. *Organometallics* **1988**, *7*, 1329. (c) Schumann, H.; Reier, F.-W.; Palamidis, E. *J. Organomet. Chem.* **1985**, *297*, C30. (d) Tilley, T. D.; Andersen, R. A.; Zalkin, R. A. *Inorg. Chem.* **1983**, *22*, 856. (e) Tilley, T. D.; Andersen, R. A.; Zalkin, R. A. *J. Am. Chem. Soc.* **1982**, *104*, 3725. (f) Bielang, G.; Fischer, R. D. *J. Organomet. Chem.* **1978**, *161*, 335 and references therein.
(7) Fryzuk, M. D.; Haddad, T. S. *J. Chem. Soc., Chem. Commun.* **1990**, 1088.
(8) (a) Fryzuk, M. D.; Rettig, S. J.; Westerhaus, A.; Williams, H. D. *Inorg. Chem.* **1985**, *24*, 4316. (b) Fryzuk, M. D.; Haddad, T. S.; Rettig, S. J. *Organometallics* **1989**, *8*, 1723. (c) Fryzuk, M. D.; Haddad, T. S.; Rettig, S. J. *J. Am. Chem. Soc.* **1990**, *112*, 8185.

0276-7333/91/2310-2026$02.50/0

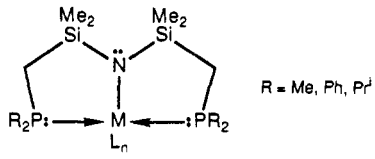

I

num as well as the lanthanide element lutetium. The synthesis, fluxional behavior, and reactivity of several bis(amido-diphosphine) complexes MCl[N-$(SiMe_2CH_2PR_2)_2]_2$ (R = Me, Pr^i, Ph; M = Y, La, Lu) are detailed; also included are the kinetics of the thermolysis reactions of some hydrocarbyl derivatives of yttrium, $YR[N(SiMe_2CH_2PMe_2)_2]_2$ (R = Ph, CH_2Ph, CD_2Ph-d_5), and the crystal structure determination of the cyclometalated product derived upon loss of hydrocarbon (RH). Some of this work has been communicated previously.[4,7]

Experimental Section

General Information. All manipulations were performed under prepurified nitrogen in a Vacuum Atmospheres HE-553-2 glovebox equipped with a MO-40-2H purification system or in standard Schlenk-type glassware on a dual vacuum/nitrogen line. Anhydrous $LaCl_3$ and YCl_3 were prepared from the oxides[9] (Aldrich), while anhydrous $LuCl_3$ was used as received (Aldrich). Phenyllithium,[10] benzylpotassium,[11] $LiN(SiMe_2CH_2PMe_2)_2$,[12] $LiN(SiMe_2CH_2PPr^i_2)_2$,[12] and $LiN(SiMe_2CH_2PPh_2)_2$[13] were prepared according to the literature procedures. $KPMe_2$ was prepared from benzylpotassium and $HPMe_2$.[14] Hexanes and THF were initially dried over CaH_2 followed by distillation from sodium–benzophenone ketyl. Ether and toluene were distilled from sodium–benzophenone ketyl. C_6D_6 and C_7D_8 were dried overnight with activated 4-Å molecular sieves, vacuum-transferred to an appropriate container, "freeze–pump–thawed" three times, and stored in the glovebox. Carbon, hydrogen, and nitrogen analyses were performed by P. Borda of this department. NMR spectra were recorded in C_6D_6 unless otherwise stated. ^1H NMR spectra (referenced to C_6D_5H at 7.15 ppm or $C_6D_5CD_2H$ at 2.09 ppm) were performed on one of the following instruments, depending on the complexity of the particular spectra: Bruker WP-80, Varian XL-300, or Bruker WH-400. ^{13}C NMR spectra (referenced to C_6D_6 at 128.0 ppm or $C_6D_5CD_3$ at 20.4 ppm) were run at 75.429 MHz ($^1J_{C-H}$ coupling constants are reported in square brackets), and ^{31}P NMR spectra (referenced to external $P(OMe)_3$ in C_6D_6 or $C_6D_5CD_3$ at 141.0 ppm) were run at 121.421 MHz, both on the XL-300 instrument. Coupling constants, J, are reported in hertz. Molecular weight determinations were carried out in C_6D_6 (at concentrations of 10–20 mg/mL) by using the isopiestic method in a Signer molecular weight apparatus.[15]

$KN(SiMe_2CH_2PMe_2)_2$. $HN(SiMe_2CH_2Cl)_2$ (3.63 mL, 16.6 mmol) was slowly added dropwise to a cooled (−10 °C) THF solution (100 mL) of $KPMe_2$ (5.00 g, 49.9 mmol) with good stirring. During the addition, the dark red color due to the phosphide faded to a pale yellow color. The THF was removed in vacuo, and the resulting glass was extracted with hexanes (150 mL) and filtered through a thick pad of Celite to remove the gelatinous KCl. Concentrating the hexanes solution and cooling to −30 °C yielded 3.50 g (66% yield) of colorless crystals of $KN(SiMe_2CH_2PMe_2)_2$. ^1H NMR: δ 1.00 (12 H, s, PMe), 0.67 (4 H, d, J = 4.2, PCH_2Si), and 0.18 (12 H, s, SiMe). $^{13}C\{^1H\}$ NMR: δ 25.92 (d, J = 20.5, PCH_2Si), 17.54 (d, J = 9.4, PMe), and 7.86 (s, SiMe). $^{31}P\{^1H\}$ NMR: δ −56.5. Anal. Calcd for $C_{10}H_{28}NP_2Si_2K$: C, 37.59; H, 8.83; N, 4.38. Found: C, 37.80; H, 9.00; N, 4.51.

$KN(SiMe_2CH_2PPh_2)_2$. $KCH_2C_6H_5$ (0.80 g, 6.14 mmol) in THF (25 mL) was slowly added dropwise to a cooled (−10 °C) THF/toluene solution (100 mL) of $HN(SiMe_2CH_2PPh_2)_2$ (3.25 g, 6.14 mmol) with good stirring. The deep orange color due to the benzylpotassium is discharged as it deprotonates the amine, leaving a yellow solution. The THF/toluene was removed in vacuo, and the resulting glass was extracted with toluene (150 mL) and filtered through Celite to remove any unreacted benzylpotassium. Concentrating the toluene solution, adding hexanes (50 mL), and cooling to −30 °C yielded 3.0 g (86% yield) of powdery $KN(SiMe_2CH_2PPh_2)_2$. ^1H NMR: δ 7.52 (8 H, m, H_o), 7.07 (12 H, m, H_m and H_p), 1.48 (4 H, d, J = 3.2, PCH_2Si), and 0.06 (12 H, s, SiMe). $^{13}C\{^1H\}$ NMR: δ 142.22 (d, J = 11.0, C_i), 132.99 (d, J = 18.6, C_o), 128.50 (d, J = 12.2, C_m), 128.49 (s, C_p), 20.29 (d, J = 26.4, PCH_2Si), and 7.82 (d, J = 3.9, SiMe). $^{31}P\{^1H\}$ NMR: δ −20.0. Anal. Calcd for $C_{30}H_{36}NP_2Si_2K$: C, 63.46; H, 6.39; N, 2.47. Found: C, 63.57; H, 6.48; N, 2.30.

$YCl[N(SiMe_2CH_2PMe_2)_2]_2$. To a slurry of YCl_3 (1.381 g, 7.07 mmol) in THF (100 mL) was added a solution of $LiN(SiMe_2CH_2PMe_2)_2$ (4.08 g, 14.20 mmol) in THF (10 mL) dropwise with good stirring. After 12 h, the THF was removed under vacuum, hexanes (50 mL) were added, and the solution was filtered through Celite to remove LiCl. Cooling a saturated hexanes solution to −30 °C gave analytically pure crystals of $YCl[N(SiMe_2CH_2PMe_2)_2]_2$ (3.60 g, yield 74%). ^1H NMR: δ 1.06 (24 H, s, PMe), 0.81 (8 H, s, PCH_2Si), and 0.35 (24 H, s, SiMe). $^{13}C\{^1H\}$ NMR: δ 20.03 (s, PCH_2Si), 15.89 (s, PMe), and 7.27 (s, SiMe). $^{31}P\{^1H\}$ NMR: δ −45.7 (d, J = 52) (see Table V and Figure 2). ^{89}Y NMR: (C_7D_8/THF): δ +449 (p, $^1J_{Y-P}$ = 52), relative to 3 M YCl_3 in D_2O at 0 ppm. Anal. Calcd for $C_{20}H_{56}ClN_2P_4Si_4Y$: C, 35.05; H, 8.24; N, 4.09. Found: C, 35.05; H, 8.30; N, 4.02. Signer molecular weight method: calcd 685 g/mol; found 635 g/mol.

$LaCl[N(SiMe_2CH_2PMe_2)_2]_2$. The same procedure as for $YCl[N(SiMe_2CH_2PMe_2)_2]_2$ was used except that 1 week of stirring at room temperature was required. $LaCl_3$ (0.38 g, 1.57 mmol) and $KN(SiMe_2CH_2PMe_2)_2$ (1.00 g, 3.13 mmol) gave 0.85 g (74% yield) of $LaCl[N(SiMe_2CH_2PMe_2)_2]_2$. NMR spectra are recorded in C_7D_8. ^1H NMR: δ 1.09 (24 H, s, PMe), 0.79 (8 H, s, PCH_2Si), and 0.27 (24 H, s, SiMe). $^{31}P\{^1H\}$ NMR: at 20 °C δ −43.51 (s); at −60 °C δ −40.42 (br, s), and −42.47 (br, s). $^{13}C\{^1H\}$ NMR: [$^1J_{C-H}$] δ 20.05 (s, PCH_2Si) [t, 118.4], 16.05 (s, PMe) [q, 127.7], and 6.81 (s, SiMe) [q, 117.1]. Anal. Calcd for $C_{20}H_{56}ClN_2P_4Si_4La$: C, 32.67; H, 7.68; N, 3.81. Found: C, 32.67; H, 7.82; N, 3.70. Signer molecular weight method: calcd 735 g/mol; found 685 g/mol.

$LuCl[N(SiMe_2CH_2PMe_2)_2]_2$. The same procedure as for $YCl[N(SiMe_2CH_2PMe_2)_2]_2$ was used. $LuCl_3$ (0.50 g, 1.79 mmol) was reacted with $LiN(SiMe_2CH_2PMe_2)_2$ (1.03 g, 3.58 mmol) to give 0.86 g (63% yield) of $LuCl[N(SiMe_2CH_2PMe_2)_2]_2$. NMR spectra are recorded in C_7D_8. ^1H NMR: δ 1.06 (24 H, s, PMe), 0.80 (8 H, s, PCH_2Si), and 0.34 (24 H, s, SiMe). $^{31}P\{^1H\}$ NMR: at 20 °C δ −42.93 (s); at −80 °C δ −40.8 (br, s). $^{13}C\{^1H\}$ NMR: [$^1J_{C-H}$] δ 20.48 (s, PCH_2Si) [t, 120.8], 16.13 (s, PMe) [q, 128.3], and 7.11 (s, SiMe) [q, 117.3]. Anal. Calcd for $C_{20}H_{56}ClN_2P_4Si_4Lu$: C, 31.14; H, 7.32; N, 3.63. Found: C, 31.34; H, 7.42; N, 3.50.

$YCl[N(SiMe_2CH_2PPr^i_2)_2]_2$. The same procedure as for $YCl[N(SiMe_2CH_2PMe_2)_2]_2$ was used. YCl_3 (0.28 g, 1.41 mmol) and $LiN(SiMe_2CH_2PPr^i_2)_2$ (1.13 g, 2.82 mmol) gave $YCl[N(SiMe_2CH_2PPr^i_2)_2]_2$. Because of the high solubility of the compound (1 g will dissolve in less than 1 mL of pentane), analytically pure material has not yet been obtained. ^1H NMR: δ 1.87 (8 H, sept, J = 7.0, PCH), 1.16 (48 H, m, PCMe), 0.91 (8 H, s, PCH_2Si), and 0.50 (24 H, s, SiMe). $^{13}C\{^1H\}$ NMR: δ 24.47 (s, $PCHMe_2$), 19.68 (t, J = 4.0, $PCHMe_2$), 11.23 (t, J = 5, PCH_2Si), and 6.00 (s, SiMe). $^{31}P\{^1H\}$ NMR: δ −1.09 (d, J = 44).

$YCl[N(SiMe_2CH_2PPh_2)_2]_2$. The same procedure as for $YCl[N(SiMe_2CH_2PMe_2)_2]_2$ was used except that the product was extracted with toluene and crystallized from toluene/hexanes. YCl_3 (0.16 g, 0.83 mmol) and $LiN(SiMe_2CH_2PPh_2)_2$ (0.89 g, 1.66 mmol) gave 0.78 g (80% yield) of $YCl[N(SiMe_2CH_2PPh_2)_2]_2$. ^1H NMR: δ 7.67 (16 H, m, H_o), 7.14 (24 H, m, H_m and H_p), 1.80 (8 H, s, PCH_2Si), and 0.33 (24 H, s, SiMe). $^{13}C\{^1H\}$ NMR: δ 138.68 (br, C_i), 133.53 (d, J = 14.1, C_o), 128.53 (d, J = 3.3, C_m), 129.10 (s, C_p), 17.43 (m, PCH_2Si), and 5.91 (s, SiMe). $^{31}P\{^1H\}$ NMR (C_7D_8): at 29 °C δ −16.3 (d, J = 39); at −59 °C −9.2 (m), −18.8 (m), −19.8 (m), and −20.6 (s) (see Figure 3). Anal. Calcd for

(9) Taylor, M. D.; Carter, C. P. *J. Inorg. Nucl. Chem.* **1962**, *24*, 387.
(10) Schlosser, M.; Ladenberger, V. *J. Organomet. Chem.* **1967**, *8*, 193.
(11) Schlosser, M.; Hartmann, J. *Angew. Chem., Int. Ed. Engl.* **1973**, *12*, 508.
(12) Fryzuk, M. D.; Carter, A.; Westerhaus, A. *Inorg. Chem.* **1985**, *24*, 642.
(13) Fryzuk, M. D.; MacNeil, P. A.; Rettig, S. J.; Secco, A. S.; Trotter, J. *Organometallics* **1982**, *1*, 918.
(14) Parshall, G. W. *Inorg. Synth.* **1968**, *11*, 157.
(15) (a) Signer, R. *Liebigs Ann. Chem.* **1930**, *478*, 246. (b) An apparatus, nearly identical with the one used in our laboratory, has recently been described: Zoellner, R. W. *J. Chem. Educ.* **1990**, *67*, 714.

$C_{60}H_{72}ClN_2P_4Si_4Y$: C, 60.98; H, 6.14; N, 2.37. Found: C, 61.02; H, 6.33; N, 2.40.

LaCl[N(SiMe$_2$CH$_2$PPh$_2$)$_2$]$_2$. The same procedure as for YCl[N(SiMe$_2$CH$_2$PPh$_2$)$_2$]$_2$ was used except that 1 week of stirring at room temperature was required. $LaCl_3$ (0.25 g, 1.01 mmol) and KN(SiMe$_2$CH$_2$PPh$_2$)$_2$ (1.15 g, 2.02 mmol) gave 0.80 g (64% yield) of LaCl[N(SiMe$_2$CH$_2$PPh$_2$)$_2$]$_2$. NMR spectra are reported in C_7D_8. ^{1}H NMR: at 80 °C δ 7.50 (16 H, s, H_o), 6.99 (24 H, s, H_m, H_p), 1.69 (8 H, s, PCH_2Si), and 0.05 (24 H, s, SiMe). ^{13}C{^{1}H} NMR: at 60 °C δ 139.05 (br, C_i), 133.71 (m, C_o), 128.58 (s, C_m), 129.06 (s, C_p), 17.59 (m, PCH_2Si), and 5.62 (s, SiMe). ^{31}P{^{1}H} NMR: at 80 °C δ −12.3 (monomer); at −39 °C δ −11.2 (s) and −19.6 (s) (dimer). In between this temperature range both species are detectable. This compound crystallizes with associated toluene. Anal. Calcd for $C_{60}H_{72}ClN_2P_4Si_4Y(C_7H_8)$: C, 60.78; H, 6.09; N, 2.12. Found: C, 60.46; H, 6.16; N, 2.03. Signer molecular weight method: calcd 1232 g/mol; found 1337 g/mol.

YPh[N(SiMe$_2$CH$_2$PMe$_2$)$_2$]$_2$. To an ether solution (25 mL) of YCl[N(SiMe$_2$CH$_2$PMe$_2$)$_2$]$_2$ (0.630 g, 0.919 mmol) was added an ether solution (5 mL) of PhLi (0.077 g, 0.916 mmol). After 20 min, the ether was removed under vacuum, the resulting oil was extracted with toluene, and the solution was filtered through Celite to remove LiCl. Addition of hexanes (1 mL) to a saturated toluene solution and cooling to −30 °C gave 0.382 g (57% yield) of colorless crystalline YPh[N(SiMe$_2$CH$_2$PMe$_2$)$_2$]$_2$. ^{1}H NMR: at 20 °C δ 8.37 (2 H, d, J = 6.9, H_o), 7.37 (2 H, t, J = 6.8, H_m), 7.22 (1 H, t, J = 6.9, H_p), 0.90 (24 H, s, PMe), 0.73 (8 H, s, PCH_2Si), and 0.41 (24 H, s, SiMe); at −49 °C in C_7D_8 δ 8.45 (H_o), 7.43 (H_m), 7.25 (H_p), 0.98, 0.95, 0.78 and 0.72 (PMe), 1.41, 0.81, 0.39 and −0.01 (PCH_2Si), and 0.64, 0.61, 0.45 and 0.18 (SiMe). ^{13}C{^{1}H} NMR: δ 191.0 (d, J = 41.5, C_i), 142.3 (s, C_o), 125.7 (s, C_m), 124.9 (s, C_p), 20.36 (s, PCH_2Si), 16.64 (s, PMe), and 7.35 (s, SiMe); at −49 °C in C_7D_8 δ 142.70 (s, C_o), 125.52 (s, C_m), 124.72 (s, C_p), 19.64 and 19.40 (s, PCH_2Si), 17.32, 16.11, 15.78 and 15.77 (s, PMe), and 8.20, 7.42, 7.21 and 6.33 (s, SiMe). ^{31}P{^{1}H} NMR: at 20 °C δ −46.7 (d, J = 43); at −49 °C δ −43.6 (m) and −48.8 (m) (see Table V and Figures 1 and 2). Anal. Calcd for $C_{26}H_{61}N_2P_4Si_4Y$: C, 42.96; H, 8.46; N, 3.85. Found: C, 43.20; H, 8.55; N, 3.81.

Y(CH$_2$C$_6$H$_5$)[N(SiMe$_2$CH$_2$PMe$_2$)$_2$]$_2$. The same procedure was followed as for the above compound except that THF was the solvent used. YCl[N(SiMe$_2$CH$_2$PMe$_2$)$_2$]$_2$ (0.500 g, 0.730 mmol) and $C_6H_5CH_2K$ (0.095 g, 0.730 mmol) gave 0.413 g (76% yield) of colorless crystalline Y(CH$_2$C$_6$H$_5$)[N(SiMe$_2$CH$_2$PMe$_2$)$_2$]$_2$. ^{1}H NMR: δ 7.22 (2 H, t, J = 7.5, H_m), 7.12 (2 H, d, J = 6.9, H_o), 6.81 (1 H, t, J = 7.2, H_p), 2.06 (2 H, br, Y−CH_2), 0.97 (24 H, s, PMe), 0.74 (8 H, s, PCH_2Si), and 0.35 (24 H, s, SiMe). ^{13}C{^{1}H} NMR: [$^1J_{C-H}$] δ 155.3 (s, C_i), 128.2 (s, C_o) [d, 154.3], 125.1 (s, C_m) [d, 152.4], 117.4 (s, C_p) [d, 158.3], 55.85 (d of q, J = −30.4 and 4.1, Y−CH_2) [t, 114.9], 20.16 (s, PCH_2Si) [t, 118.5], 16.64 (s, PMe) [q, 128.2], and 7.35 (s, SiMe) [q, 117.2]. ^{31}P{^{1}H} NMR: δ −46.7 (d, J = 43). Anal. Calcd for $C_{27}H_{63}N_2P_4Si_4Y$: C, 43.77; H, 8.57; N, 3.78. Found: C, 43.56; H, 8.70; N, 3.60.

LuPh[N(SiMe$_2$CH$_2$PMe$_2$)$_2$]$_2$. The same procedure as for the yttrium analogue was used. LuCl[N(SiMe$_2$CH$_2$PMe$_2$)$_2$]$_2$ (0.205 g, 0.266 mmol) and C_6H_5Li (0.023 g, 0.27 mmol) gave 0.19 g (87% yield) of colorless crystalline LuPh[N(SiMe$_2$CH$_2$PMe$_2$)$_2$]$_2$. NMR spectra are reported in C_7D_8. ^{1}H NMR: at 20 °C δ 8.24 (2 H, d, J = 6.6, H_o), 7.28 (2 H, t, J = 7.2, H_m), 7.11 (1 H, t, J = 7.2, H_p), 0.94 (24 H, s, PMe), 0.68 (8 H, s, PCH_2Si), and 0.37 (24 H, s, SiMe); at −70 °C δ 8.52 (H_o), 7.50 (H_m), 7.28 (H_p), 0.98, 0.95, 0.76 and 0.76 (PMe), 1.39, 0.80, 0.39 and −0.73 (PCH_2Si), and 0.71, 0.65, 0.49 and 0.20 (SiMe). ^{31}P{^{1}H} NMR: at 20 °C δ −43.58 (s); at −59 °C δ −39.69 (m) and −46.40 (m) (see Table V and Figure 2). ^{13}C{^{1}H} NMR: at 20 °C δ 195 (s, C_i), 142.77 (s, C_o), 125.96 (s, C_m), 124.98 (s, C_p), 20.10 (s, PCH_2Si), 16.99 (s, PMe), and 7.35 (s, SiMe); at −49 °C δ 195.5 (C_i), 143.83 (C_o), 125.73 (C_m), 124.73 (C_p), 20.05 and 19.56 (PCH_2Si), 17.68, 16.61, 16.34 and 16.21 (PMe), and 8.20, 7.78, 7.16 and 6.68 (SiMe). Anal. Calcd for $C_{20}H_{56}ClN_2P_4Si_4Y$: C, 35.05; H, 8.24; N, 4.09. Found: C, 35.05; H, 8.30; N, 4.02.

Y[N(SiMe$_2$CHPMe$_2$)(SiMe$_2$CH$_2$PMe$_2$)][N(SiMe$_2$CH$_2$PMe$_2$)$_2$]. Thermolysis of Y(CH$_2$C$_6$H$_5$)[N(SiMe$_2$CH$_2$PMe$_2$)$_2$]$_2$ or YPh[N(SiMe$_2$CH$_2$PMe$_2$)$_2$]$_2$ in toluene results in quantitative conversion to this cyclometalated product. This compound is exceedingly soluble in pentane and has only been isolated in very low yield. ^{1}H NMR: in C_7D_8 at −38 °C of this compound consists of sharp resonances between δ 1.35 and 0.92 (PMe and YCHP), multiplets between δ 0.85 and 0.40 (PCH_2Si, some are obscured), and 0.49, 0.38, 0.37, 0.34, 0.33, 0.29, 0.23, and 0.22 (8 SiMe). ^{13}C{^{1}H} NMR: in C_7D_8 at −28 °C δ 32.29 (d of d, J = 44.7 and 9.3, YCHP), 22.17, 21.41, and 20.3 (3 PCH_2Si), 18.82, 18.50, 18.40, 17.43, 16.16, 15.77, 15.53, and 14.80 (8 PMe), and 10.03, 8.29, 7.59, 7.35, 7.14, 6.99, 6.76, and 5.63 (8 SiMe). ^{31}P{^{1}H} NMR: in C_7D_8 at −29 °C four multiplets at δ −34.2, −41.9, −42.0, and −45.3 (see Table VI and Figure 4). ^{89}Y NMR (C_7D_8): δ +533 (multiplet due to ^{31}P coupling), relative to 3 M YCl_3 in D_2O at 0 ppm. Anal. Calcd for $C_{20}H_{55}N_2P_4Si_4Y$: C, 37.02; H, 8.54; N, 4.32. Found: C, 37.41; H, 8.54; N, 4.22.

Lu[N(SiMe$_2$CHPMe$_2$)(SiMe$_2$CH$_2$PMe$_2$)][N(SiMe$_2$CH$_2$PMe$_2$)$_2$]. This compound can be quantitatively formed from the phenyl derivative **6a** as described for yttrium. It too has only been isolated in low yield due to its extreme solubility in pentane. ^{1}H NMR of this compound consists of sharp resonances between δ 1.35 and 0.93 (PMe and LuCHP), multiplets between δ 0.82 and 0.40 (PCH_2Si), and 0.41, 0.33, 0.31, 0.29, 0.27, 0.24, 0.21, and 0.20 (8 SiMe). ^{13}C{^{1}H} NMR: in C_7D_8 at −28 °C δ 34.03 (d of t, J = 43.6 and 4, LuCHP), 30.19, 22.77, and 20.0 (3 PCH_2Si), resonances from 21 to 15 (8 PMe), and 10.36, 7.83, 7.72, 7.43, 7.17, 6.78, 6.55, and 5.69 (8 SiMe). ^{31}P{^{1}H} NMR: δ −34.8 (m), −36.1 (m), −38.6 (m), and −40.1 (m) (see Table VI). Anal. Calcd for $C_{20}H_{55}N_2P_4Si_4Lu$: C, 32.69; H, 7.54; N, 3.81. Found: C, 33.20; H, 7.57; N, 3.42.

La[N(SiMe$_2$CHPMe$_2$)(SiMe$_2$CH$_2$PMe$_2$)][N(SiMe$_2$CH$_2$PMe$_2$)$_2$]. To a hexane solution (50 mL) of LaCl[N(SiMe$_2$CH$_2$PMe$_2$)$_2$]$_2$ (0.615 g, 0.836 mmol) was added a hexane solution (10 mL) of $LiCH_2SiMe_3$ (79 mg, 0.84 mmol) dropwise, with good stirring. The mixture immediately became both cloudy (due to the formation of LiCl) and bright yellow (due to metalation of the ligand) in appearance. After stirring for 2 h, the solution was filtered through Celite and the filtrate was evaporated to dryness to remove $SiMe_4$. The crude crystalline product was redissolved in a few milliliters of hexanes and cooled to −30 °C to give 0.395 g of product (68% yield). NMR spectra are reported in $CD_3C_6D_5$. ^{1}H NMR: at 20 °C δ 1.30 (d, J = 6, PMe_2), 1.24 (m, PCH(Y)(Si)), 1.03 (s, 2 PMe_2), 1.01 (d, J = 4, PMe_2), 0.90 (m, PCH_2Si), 0.68 (m, 2 PCH_2Si), 0.28 (s, $SiMe_2$), 0.17 (s, $SiMe_2$), and 0.14 (s, 2 $SiMe_2$). ^{31}P{^{1}H} NMR: at −99 °C δ −21.3 (d, J = 27), −35.5 (broad), −37.3 (very broad), and −38.3 (d, J = 27). Anal. Calcd for $C_{20}H_{55}N_2P_4Si_4La$: C, 34.33; H, 7.92; N, 4.00. Found: C, 34.05; H, 7.94; N, 4.00.

Kinetics of the Thermolysis Reactions. The first-order decomposition of M(R)[N(SiMe$_2$CH$_2$PMe$_2$)$_2$] was monitored with ^{31}P{^{1}H} NMR spectroscopy by following the disappearance of the hydrocarbyl complex over time. In order to ensure accurate integrations, a 12-s delay between 20° pulses was utilized. Typically, the spectra were collected at room temperature on sealed 0.09 mol/L C_6D_6 solutions in sealed NMR tubes. These samples were immersed in an oil bath (maintained at a specific temperature) for a known length of time, and the reaction was quenched by freezing the sample. For the benzyl-d_0 and -d_7 compounds, the samples were treated identically: each sample spent exactly the same length of time immersed in the oil bath, frozen, and monitored in the spectrometer.

X-ray Crystallographic Analysis Y[N(SiMe$_2$CHPMe$_2$)(SiMe$_2$CH$_2$PMe$_2$)][N(SiMe$_2$CH$_2$PMe$_2$)$_2$]. Crystallographic data appear in Table I. The final unit cell parameters were obtained by least squares on the setting angles for 25 reflections with 2θ = 51.5–69.9°. The intensities of three standard reflections, measured every 150 reflections throughout the data collection, showed only small random variations. The data were processed and corrected for Lorentz and polarization effects and absorption (empirical, based on azimuthal scans for four reflections).[16]

The structure was solved by conventional heavy-atom methods, the coordinates of the Y atom being determined from the Pat-

(16) TEXSAN/TEXRAY structure analysis package which includes versions of the following: DIRDIF, direct methods for difference structures, by P. T. Beurskens; ORFLS, full-matrix least-squares, and ORFFE, function and errors, by W. R. Busing, K. O. Martin, and H. A. Levy; ORTEP II, illustrations, by C. K. Johnson.

Table I. Crystallographic Data[a]

compd	$Y[N(SiMe_2CHPMe_2)(SiMe_2CH_2PMe_2)][N(SiMe_2CH_2PMe_2)_2]$
formula	$C_{20}H_{55}N_2P_2Si_4Y$
fw	648.81
color, habit	colorless, plate
cryst size, mm	0.05 × 0.25 × 0.40
cryst syst	monoclinic
space group	$P2_1/c$
a, Å	18.115 (1)
b, Å	15.875 (8)
c, Å	12.706 (2)
β, deg	92.619 (7)
V, Å^3	3650 (2)
Z	4
T, °C	21
ρ_c, g/cm^3	1.181
$F(000)$	1376
radiation	Cu
wavelength, Å	1.541 78
μ, cm^{-1}	53.6
transm factors	0.32–1.00
scan type	ω–2θ
scan range, deg in ω	0.89 + 0.30 tan θ
scan speed, deg/min	32
data collcd	$+h,+k,\pm l$
$2\theta_{max}$, deg	155
cryst decay	negligible
total no. of reflns	7955
no. of unique reflns	7724
R_{int}	0.056
no. of reflns with $I \geq 3\sigma(I)$	3270
no. of variables	281
R	0.063
R_w	0.073
gof	2.16
max Δ/σ (final cycle)	0.10
residual density, e/Å^3	−0.89, +1.42 (both near Y)

[a] Temperature 294 K, Rigaku AFC6S diffractometer, graphite monochromator, take-off angle 6.0°, aperture 6.0 × 6.0 mm at a distance of 285 mm from the crystal, stationary background counts at each end of the scan (scan:background time ratio 2:1), $\sigma^2(F^2) = [S^2(C + 4B) + (0.035F^2)^2]/Lp^2$ (S = scan speed, C = scan count, B = normalized background count), function minimized $\sum w(|F_o| - |F_c|)^2$ where $w = 4F_o^2/\sigma^2(F_o^2)$, $R = \sum||F_o| - |F_c||/\sum|F_o|$, $R_w = (\sum w(|F_o| - |F_c|)^2/\sum w|F_o|^2)^{1/2}$, and gof = $[\sum(|F_o| - |F_c|)^2/(m - n)]^{1/2}$. Values given for R, R_w, and gof are based on those reflections with $I \geq 3\sigma(I)$.

terson function and those of the remaining non-hydrogen atoms from subsequent difference Fourier syntheses. All non-hydrogen atoms were refined with anisotropic thermal parameters. Hydrogen atoms were fixed in idealized positions (C–H = 0.98 Å, $B_H = 1.2B$(bonded atom)). A correction for secondary extinction was applied, the final value of the extinction coefficient being 1.77 × 10^{-6}. Neutral-atom scattering factors and anomalous dispersion corrections for the non-hydrogen atoms were taken from ref 17. Final atomic coordinates and equivalent isotropic thermal parameters, bond lengths, and bond angles appear in Tables II–IV, respectively. Hydrogen atom parameters, anisotropic thermal parameters, torsion angles, intermolecular contacts, least-squares planes, and measured and calculated structure factor amplitudes are included as supplementary material.

Results and Discussion

Synthetic Considerations. The synthesis of bis(amido–diphosphine) complexes $MCl[N(SiMe_2CH_2PR_2)_2]_2$ (M = Y, La, Lu) is relatively straightforward. Addition of 2 equiv of the lithium amides to YCl_3 or $LuCl_3$ (eq 1) or 2 equiv of the potassium amides to $LaCl_3$ (eq 2) in THF generates the desired compounds in good yields. The

$$\underset{M = Y, Lu}{MCl_3} + 2LiN(SiMe_2CH_2PR_2)_2 \xrightarrow[THF]{24\ h} MCl[N(SiMe_2CH_2PR_2)_2]_2 + 2LiCl \quad (1)$$

M = Y: R = Me (**1a**), Ph (**1b**), Pr^i (**1c**)
M = Lu: R = Me (**2a**)

$$LaCl_3 + 2KN(SiMe_2CH_2PR_2)_2 \xrightarrow[THF]{7\ days} LaCl[N(SiMe_2CH_2PR_2)_2]_2 + 2KCl \quad (2)$$

R = Me (**3a**), Ph (**3b**)

choice of lithium versus potassium salts of the ligand seems to be a function of the size of the metal; for the smaller elements Lu and Y (M^{3+} ionic radii of 1.00 and 1.04 Å, respectively),[18] either amide salt will generate good yields of bis(ligand) complex. However, the trichloride of the larger metal La (La^{3+} ionic radius of 1.17 Å)[18] does not react with any of the lithium amides; the use of the potassium salts and long reaction times are required to obtain the phosphine complexes. This dependence on the alkali-metal salt is reminiscent of the preparation of metallocene derivatives of the lanthanides.[19]

A range of substituents at phosphorus have been employed. While most of the discussion on reactivity and fluxional behavior will focus on those complexes having methyl groups on phosphorus (–PMe_2: **a** series), phenyl substituents (–PPh_2: **b** series) have also been utilized, although as will be discussed later, these show quite different fluxional behavior from the a series. Isopropyl substituents (–PPr^i_2: **c** series) were also investigated and found to generate phosphine complexes, as evidenced by $^{31}P\{^1H\}$ NMR spectroscopy, but little success was encountered in purifying these materials because of their high solubility.

The remaining chloride ligand on those complexes with methyl substituents at phosphorus, $MCl[N(SiMe_2CH_2PMe_2)_2]_2$ (**1a–3a**), can be further derivatized to generate hydrocarbyl derivatives that are stable under nitrogen indefinitely as crystalline solids (except for M = La, eq 3). While a number of reagents have been utilized

$$MCl[N(SiMe_2CH_2PMe_2)_2]_2 + \underset{RM' = PhLi,\ PhCH_2K}{RM'} \xrightarrow{THF} MR[N(SiMe_2CH_2PMe_2)_2]_2 + M'Cl \quad (3)$$

M = Y: R = Ph (**4a**), $PhCH_2$ (**5a**)
M = Lu: R = Ph (**6a**)

to metathesize the chloride, only phenyllithium and benzyl potassium gave tractable materials; the use of Grignard reagents results in displacement of one of the ligands, but not the chloride.[20]

In solution these hydrocarbyl compounds are thermally labile and cleanly undergo a cyclometalation reaction via abstraction of a methylene proton ($PC\underline{H}_2Si$) from the ligand backbone with extrusion of hydrocarbon (eq 4). For

$$MR[N(SiMe_2CH_2PMe_2)_2]_2 \xrightarrow{\Delta} M[N(SiMe_2\underline{C}HPMe_2)(SiMe_2CH_2PMe_2)][N(SiMe_2CH_2PR_2)_2] + R\text{–}H \quad (4)$$

M = Y (**7a**), Lu (**8a**), La (**9a**)

(17) International tables for X-ray crystallography; Kynoch Press: Birmingham, UK, 1974; Vol. IV, pp 99–102 and 149 (present distributor D. Reidel: Dordrecht, The Netherlands).

(18) Shannon, R. D. *Acta Crystallogr.* **1976**, *A32*, 751.

(19) Tilley, T. D.; Andersen, R. A.; Spencer, B.; Ruben, H.; Zalkin, A.; Templeton, D. H. *Inorg. Chem.* **1980**, *19*, 2999.

(20) Fryzuk, M. D.; Haddad, T. D.; Rettig, S. J. Manuscript in preparation.

Table II. Positional Parameters and *B*(eq) Values

atom	*x*	*y*	*z*	*B*(eq), Å²
Y(1)	0.25215 (4)	0.51693 (6)	0.22160 (7)	4.27 (4)
P(1)	0.3611 (1)	0.3742 (2)	0.2363 (2)	4.9 (1)
P(2)	0.1913 (2)	0.6800 (2)	0.2297 (3)	6.0 (2)
P(3)	0.2156 (1)	0.4535 (2)	0.0119 (2)	4.7 (1)
P(4)	0.2449 (2)	0.5025 (2)	0.4487 (2)	6.2 (2)
Si(1)	0.4476 (1)	0.5377 (2)	0.2740 (2)	4.8 (1)
Si(2)	0.3510 (1)	0.6610 (2)	0.1454 (2)	4.8 (1)
Si(3)	0.1256 (1)	0.3467 (2)	0.1621 (2)	4.6 (1)
Si(4)	0.0940 (2)	0.4540 (2)	0.3451 (2)	5.3 (2)
N(1)	0.3672 (4)	0.5710 (5)	0.2184 (6)	4.2 (4)
N(2)	0.1467 (4)	0.4286 (5)	0.2431 (6)	4.3 (4)
C(1)	0.4319 (5)	0.4251 (7)	0.3178 (8)	5.6 (6)
C(2)	0.2496 (5)	0.6659 (7)	0.1270 (8)	5.8 (6)
C(3)	0.1858 (5)	0.3484 (6)	0.0430 (8)	5.3 (5)
C(4)	0.1466 (6)	0.5180 (8)	0.4462 (9)	6.9 (7)
C(5)	0.4082 (6)	0.3532 (8)	0.116 (1)	7.6 (7)
C(6)	0.3552 (6)	0.2684 (8)	0.292 (1)	8.8 (8)
C(7)	0.1013 (6)	0.702 (1)	0.167 (1)	10 (1)
C(8)	0.2080 (8)	0.782 (1)	0.301 (1)	11 (1)
C(9)	0.1323 (7)	0.5027 (8)	−0.043 (1)	8.2 (8)
C(10)	0.2696 (7)	0.4429 (9)	−0.1048 (9)	7.5 (7)
C(11)	0.2854 (8)	0.576 (1)	0.546 (1)	12 (1)
C(12)	0.2577 (7)	0.404 (1)	0.517 (1)	10 (1)
C(13)	0.5267 (6)	0.5379 (9)	0.184 (1)	8.5 (8)
C(14)	0.4802 (6)	0.5987 (8)	0.393 (1)	7.8 (8)
C(12)	0.3983 (6)	0.7542 (7)	0.205 (1)	7.5 (7)
C(16)	0.3870 (7)	0.6545 (9)	0.009 (1)	8.1 (8)
C(17)	0.1426 (6)	0.2408 (7)	0.2242 (9)	6.4 (6)
C(18)	0.0273 (5)	0.3452 (8)	0.1103 (9)	6.5 (7)
C(19)	0.0096 (6)	0.517 (1)	0.306 (1)	9.0 (8)
C(20)	0.0583 (6)	0.3599 (9)	0.418 (1)	8.1 (8)

Table III. Intramolecular Distances[a]

Y(1)–N(1)	2.256 (7)	P(4)–C(11)	1.83 (1)
Y(1)–N(2)	2.396 (7)	Si(1)–N(1)	1.675 (7)
Y(1)–C(2)	2.65 (1)	Si(1)–C(14)	1.87 (1)
Y(1)–P(2)	2.817 (3)	Si(1)–C(13)	1.88 (1)
Y(1)–P(3)	2.896 (3)	Si(1)–C(1)	1.90 (1)
Y(1)–P(4)	2.903 (3)	Si(2)–N(1)	1.721 (8)
Y(1)–P(1)	3.005 (3)	Si(2)–C(2)	1.84 (1)
P(1)–C(1)	1.80 (1)	Si(2)–C(15)	1.86 (1)
P(1)–C(5)	1.82 (1)	Si(2)–C(16)	1.88 (1)
P(1)–C(6)	1.83 (1)	Si(3)–N(2)	1.690 (8)
P(2)–C(2)	1.73 (1)	Si(3)–C(18)	1.87 (1)
P(2)–C(7)	1.81 (1)	Si(3)–C(17)	1.88 (1)
P(2)–C(8)	1.86 (2)	Si(3)–C(3)	1.91 (1)
P(3)–C(3)	1.80 (1)	Si(4)–N(2)	1.692 (7)
P(3)–C(9)	1.81 (1)	Si(4)–C(4)	1.86 (1)
P(3)–C(10)	1.82 (1)	Si(4)–C(19)	1.88 (1)
P(4)–C(4)	1.80 (1)	Si(4)–C(20)	1.89 (1)
P(4)–C(12)	1.80 (2)		

[a] Distances are in angstroms. Estimated standard deviations in the least significant figure are given in parentheses.

the corresponding lanthanum complex LaCl[N-($SiMe_2CH_2PME_2$)$_2$]$_2$, reaction with phenyllithium yielded only the cyclometalated complex; this particular phenyl derivative could not be observed at room temperature.

It is noteworthy that while all the syntheses and some of the reactivity studies were performed in THF, a solvent which is well-known to bind to group 3 metal complexes and derivatives of the lanthanides,[21] no coordination by THF is observed in any of these reactions. It would appear that these bis(ligand) chloro and hydrocarbyl complexes are coordinatively saturated.

Spectral Characterization and Fluxional Behavior. All of the seven-coordinate chloro and hydrocarbyl complexes are fluxional in solution as expected.[22] As has been previously discussed,[4,7] the compounds MCl[N-($SiMe_2CH_2PMe_2$)$_2$]$_2$ (**1a–3a**) display temperature-dependent NMR behavior. Thus at room temperature each complex displays very simple NMR spectra consisting of three resonances in each of the appropriate $^{13}C\{^1H\}$ and ^1H NMR regions for the phosphorus methyl hydrogens and carbons, the methylene protons and carbons, and the silyl methyl hydrogens and carbons, respectively. At low temperatures, the ^1H NMR spectra of these chloro derivatives are uninformative, as broad signals are observed right down to −95 °C. However, the low-temperature ^1H NMR spectra of the yttrium and lutetium phenyl complexes, **4a** and **6a**, respectively, display proton resonances for four different silyl methyls, four phosphorus methyls, and four methylene groups, while the low-temperature $^{13}C\{^1H\}$ NMR spectra show four silyl–methyl, four phosphorus–methyl, and two methylene carbon resonances; resonances due to the phenyl moiety are also observed but provide no information on fluxionality.

Similar results are obtained from the $^{31}P\{^1H\}$ NMR spectra. At room temperature the spectra of the chloro and phenyl derivatives, **1a–3a** and **4a** and **6a**, respectively, show only one phosphorus resonance (a doublet for the spin-active ^{89}Y derivatives and a singlet for the lutetium and lanthanum complexes) indicative of fast exchange of the phosphorus donor environments. As the temperature is lowered, the signal broadens and gradually decoalesces into two resonances, which implies two chemically inequivalent sites in the slow-exchange limit. Of the chloro derivatives **1a–3a**, only the yttrium complex **1a** generates

Table IV. Intramolecular Bond Angles[a]

N(1)–Y(1)–N(2)	165.2 (3)	C(4)–P(4)–Y(1)	93.5 (4)
N(1)–Y(1)–C(2)	69.5 (3)	C(12)–P(4)–C(11)	101.0 (8)
N(1)–Y(1)–P(2)	90.9 (2)	C(12)–P(4)–Y(1)	122.4 (5)
N(1)–Y(1)–P(3)	106.7 (2)	C(11)–P(4)–Y(1)	126.0 (5)
N(1)–Y(1)–P(4)	97.6 (2)	N(1)–Si(1)–C(14)	114.5 (5)
N(1)–Y(1)–P(1)	71.5 (2)	N(1)–Si(1)–C(13)	114.5 (5)
N(2)–Y(1)–C(2)	125.2 (3)	N(1)–Si(1)–C(1)	106.4 (4)
N(2)–Y(1)–P(2)	102.6 (2)	C(14)–Si(1)–C(13)	105.8 (6)
N(2)–Y(1)–P(3)	75.6 (2)	C(14)–Si(1)–C(1)	107.2 (5)
N(2)–Y(1)–P(4)	76.6 (2)	C(13)–Si(1)–C(1)	108.1 (5)
N(2)–Y(1)–P(1)	94.4 (2)	N(1)–Si(2)–C(2)	104.4 (4)
C(2)–Y(1)–P(2)	36.7 (2)	N(1)–Si(2)–C(15)	112.2 (4)
C(2)–Y(1)–P(3)	83.9 (2)	N(1)–Si(2)–C(16)	113.1 (5)
C(2)–Y(1)–P(4)	121.3 (2)	C(2)–Si(2)–C(15)	117.2 (5)
C(2)–Y(1)–P(1)	134.3 (2)	C(2)–Si(2)–C(16)	105.8 (5)
P(2)–Y(1)–P(3)	106.2 (1)	C(15)–Si(2)–C(16)	104.3 (6)
P(2)–Y(1)–P(4)	90.0 (1)	N(2)–Si(3)–C(18)	114.1 (5)
P(2)–Y(1)–P(1)	161.38 (9)	N(2)–Si(3)–C(17)	113.9 (4)
P(3)–Y(1)–P(4)	150.2 (1)	N(2)–Si(3)–C(3)	110.6 (4)
P(3)–Y(1)–P(1)	85.24 (8)	C(18)–Si(3)–C(17)	105.8 (5)
P(4)–Y(1)–P(1)	86.5 (1)	C(18)–Si(3)–C(3)	106.9 (5)
C(1)–P(1)–C(5)	102.5 (5)	C(17)–Si(3)–C(3)	105.0 (5)
C(1)–P(1)–C(6)	104.2 (6)	N(2)–Si(4)–C(4)	111.7 (4)
C(1)–P(1)–Y(1)	98.4 (4)	N(2)–Si(4)–C(19)	113.9 (5)
C(5)–P(1)–C(6)	101.2 (6)	N(2)–Si(4)–C(20)	113.8 (5)
C(5)–P(1)–Y(1)	114.7 (4)	C(4)–Si(4)–C(19)	106.1 (6)
C(6)–P(1)–Y(1)	131.9 (4)	C(4)–Si(4)–C(20)	105.6 (6)
C(2)–P(2)–C(7)	105.2 (6)	C(19)–Si(4)–C(20)	105.0 (6)
C(2)–P(2)–C(8)	112.6 (6)	Si(1)–N(1)–Si(2)	127.8 (4)
C(2)–P(2)–Y(1)	66.5 (4)	Si(1)–N(1)–Y(1)	131.2 (4)
C(7)–P(2)–C(8)	99.6 (7)	Si(2)–N(1)–Y(1)	101.0 (3)
C(7)–P(2)–Y(1)	120.5 (5)	Si(3)–N(2)–Si(4)	122.0 (4)
C(8)–P(2)–Y(1)	139.2 (5)	Si(3)–N(2)–Y(1)	122.6 (4)
C(3)–P(3)–C(9)	103.3 (5)	Si(4)–N(2)–Y(1)	115.3 (4)
C(3)–P(3)–C(10)	105.6 (6)	P(1)–C(1)–Si(1)	111.5 (5)
C(3)–P(3)–Y(1)	100.3 (3)	P(2)–C(2)–Si(2)	123.3 (6)
C(9)–P(3)–C(10)	101.4 (6)	P(2)–C(2)–Y(1)	76.8 (4)
C(9)–P(3)–Y(1)	110.8 (5)	Si(2)–C(2)–Y(1)	84.7 (4)
C(10)–P(3)–Y(1)	132.3 (4)	P(3)–C(3)–Si(3)	112.0 (5)
C(4)–P(4)–C(12)	103.5 (6)	P(4)–C(4)–Si(4)	114.3 (6)
C(4)–P(4)–C(11)	106.9 (6)		

[a] Angles are in degrees. Estimated standard deviations in the least significant figure are given in parentheses.

(21) Evans, W. J.; Grate, J. W.; Choi, H. W.; Bloom, I.; Hunter, W. E.; Atwood, J. L. *J. Am. Chem. Soc.* **1985**, *107*, 941.
(22) Drew, M. G. B. *Prog. Inorg. Chem.* **1977**, *23*, 67.

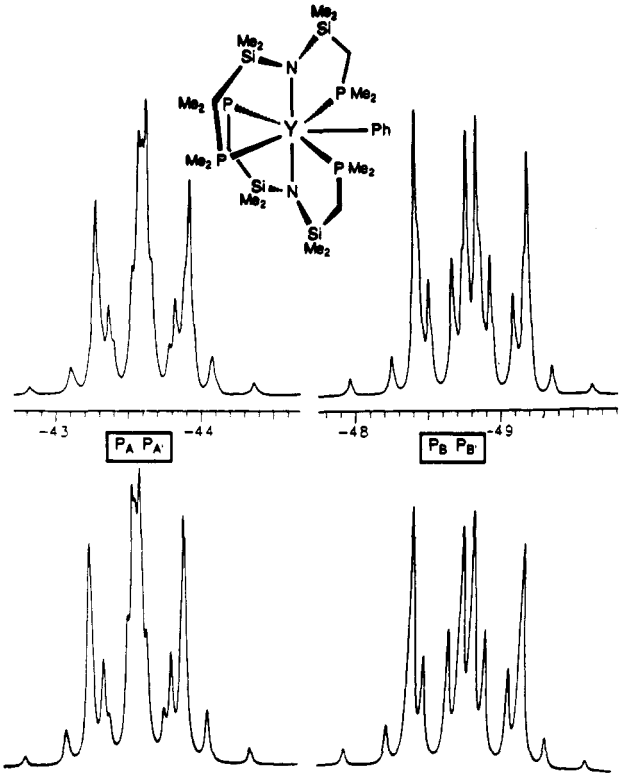

Figure 1. 121-MHz $^{31}P\{^1H\}$ NMR spectrum of YPh[N(SiMe$_2$CH$_2$PMe$_2$)$_2$]$_2$ in $C_6D_5CD_3$ recorded at −49 °C (top) and a simulation (bottom) using Bruker PANIC software. See Figure 2 and Table V for details.

Table V. $^2J_{P-P}$ and $^1J_{P-Y}$ Coupling Constants for MR'[N(SiMe$_2$CH$_2$PMe$_2$)$_2$]$_2$

coupling	M = Y, R' = Ph[a]	M = Lu, R' = Ph[b]	M = Y, R' = Cl[c]
$^2J_{P_A-P_{A'}}$	±21.9	±19.6	±18.0
$^2J_{P_A-P_B}$	−6.3	−7.85	−2.0
$^2J_{P_A-P_{B'}}$	+49.1	+70.75	+49.0
$^2J_{P_{A'}-P_B}$	+49.1	+70.75	+49.0
$^2J_{P_{A'}-P_{B'}}$	−6.3	−7.85	−2.0
$^2J_{P_B-P_{B'}}$	±44.1	±62.1	±80.0
$^1J_{P_A-Y}$	36.5		52.3
$^1J_{P_{A'}-Y}$	36.5		52.3
$^1J_{P_B-Y}$	51.3		50.8
$^1J_{P_{B'}-Y}$	51.3		50.8

[a] At −49 °C: $\delta(P_A) = \delta(P_{A'}) = -43.6$ ppm, $\delta(P_B) = \delta(P_{B'}) = -48.8$ ppm. [b] At −59 °C: $\delta(P_A) = \delta(P_{A'}) = -39.7$ ppm, $\delta(P_B) = \delta(P_{B'}) = -46.4$ ppm. [c] At −90 °C: $\delta(P_A) = \delta(P_{A'}) = -43.8$ ppm, $\delta(P_B) = \delta(P_{B'}) = -45.9$ ppm.

an analyzable pattern, while the remaining show two somewhat broadened signals. On the other hand, the yttrium- and lutetium-phenyl complexes **4a** and **6a** display well-resolved second-order spectra that can be analyzed as AA'BB'X for spin $^1/_2$ ^{89}Y and AA'BB' for Lu spin systems, respectively. The experimental and simulated patterns for YPh[N(SiMe$_2$CH$_2$PMe$_2$)$_2$]$_2$ (**4a**) at −49 °C are shown in Figure 1, while the couplings are tabulated in Table V.

Assigning the structure of these complexes in the low-temperature limit as a pentagonal bipyramid with C_2 or C_s symmetry satisfies the observed NMR data. The three possible geometrical isomers that fulfill these requirements are shown in Figure 2. The relative disposition of the tridentate amido–diphosphine ligands could be *fac–fac* (C_2 symmetry where the phosphine donors of each ligand are cisoid across the pentagonal plane), *mer–mer* (C_2 symmetry where the phosphine donors of each ligand are transoid across the pentagonal plane), or *fac–mer* (C_s symmetry

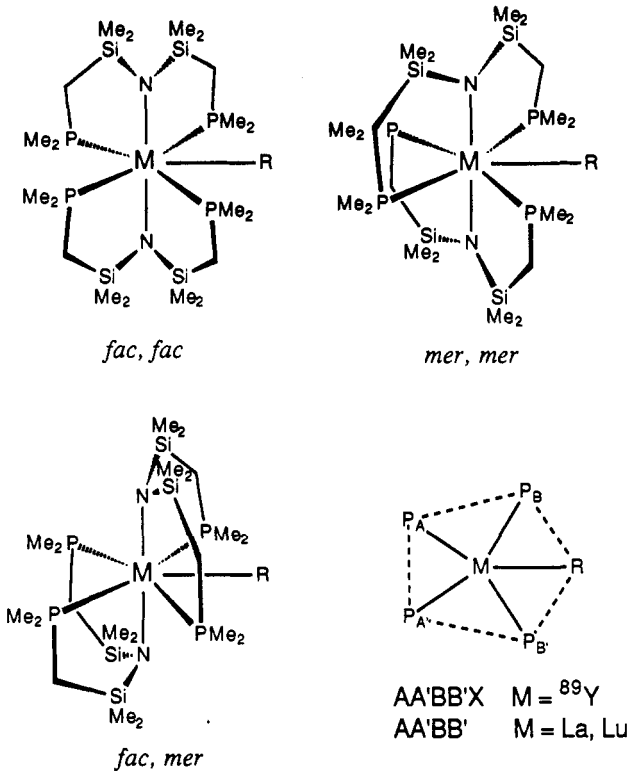

Figure 2. Possible geometric isomers for the bis(ligand) derivatives MR[N(SiMe$_2$CH$_2$PMe$_2$)$_2$]$_2$. Also included are the $^{31}P\{^1H\}$ NMR spin systems for the phosphorus nuclei assuming that all the phosphorus donors are in the equatorial plane of the pentagonal bipyramid. Refer to Figure 1 and Table V for details.

where phosphine donors of one ligand are transoid and the other are cisoid). At this point we are unable to distinguish among these possibilities, but the *mer–mer* arrangement of the ligands is the most reasonable for the low-temperature limit, as it would introduce the least steric strain in the N(SiMe$_2$R)$_2$ unit of each tridentate ligand.

Further indirect evidence for the assumed low-temperature-limiting pentagonal-bipyramidal geometry is that the magnitudes of the two-bond phosphorus–phosphorus couplings ($^2J_{P-P}$) correlate with the assumed positions in the equatorial pentagonal plane in that transoid couplings are greater than cisoid ones. For example, as given in Table V, $^2J_{P_A-P_{A'}}$, a cisoid coupling, is smaller than any of the transoid couplings, $^2J_{P_A-P_{B'}}$, $^2J_{P_{A'}-P_B}$, and $^2J_{P_B-P_{B'}}$. These transoid couplings also correlate with previously reported[8b] $^2J_{P-P}$ values of 53–80 Hz for trans-disposed phosphines in the group 4 complexes MR(η^4-C$_4$H$_6$)[N(SiMe$_2$CH$_2$PMe$_2$)$_2$] (M = Zr, Hf; R = Cl, Ph, Np).

To account for the fluxional behavior of these phosphine complexes in solution, one is tempted to invoke pseudorotation or stereochemical nonrigidity, a known feature of many seven-coordinate complexes.[22] However, a simpler explanation is that these processes occur by rapid equilibria involving dissociation of the phosphine arms of the tridentate ligands followed by reassociation. There is little variance in the free energy of activation, $\Delta G^{\ddagger}$, of the chloro complexes MCl[N(SiMe$_2$CH$_2$PMe$_2$)$_2$]$_2$ (**1a–3a**) for the process that renders all four phosphines equivalent: $\Delta G^{\ddagger}$ changes only slightly from 10.1 kcal/mol for M = Y to 10 kcal/mol for M = La to 9 kcal/mol for M = Lu. Analogous results are obtained for the phenyl derivatives, MPh[N(SiMe$_2$CH$_2$PMe$_2$)$_2$]$_2$ (**4a** and **6a**), for which the $\Delta G^{\ddagger}$'s are also very similar, ranging from 11.5 kcal/mol for M = Y to 11.0 kcal/mol for M = Lu.

When the substituents at phosphorus are changed from methyl to phenyl, to generate a bulkier, less basic donor

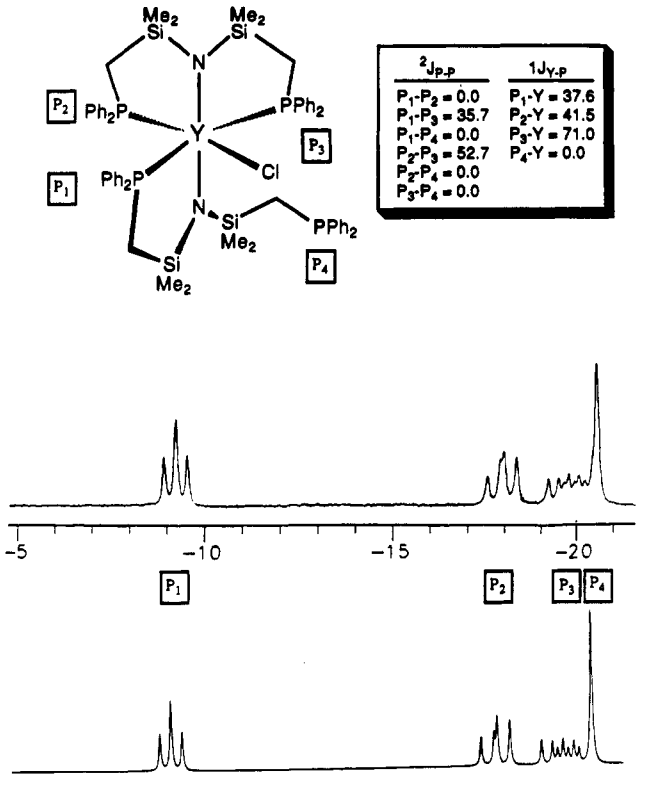

Figure 3. 121-MHz $^{31}P\{^1H\}$ NMR spectrum of YCl[N(SiMe$_2$CH$_2$PPh$_2$)$_2$]$_2$ in $C_6D_5CD_3$ recorded at −59 °C (top) and a simulation (bottom) using Bruker PANIC software.

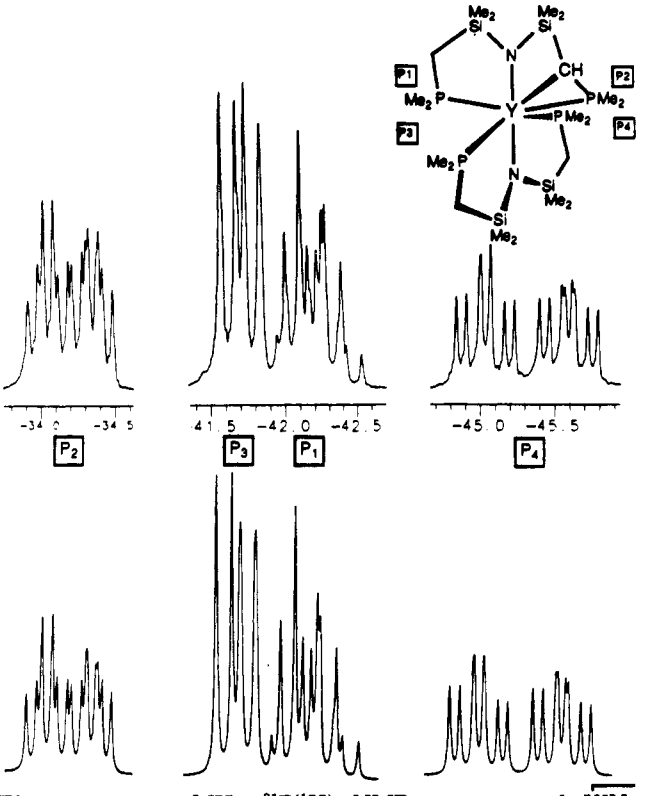

Figure 4. 121-MHz $^{31}P\{^1H\}$ NMR spectrum of Y[N(SiMe$_2$CHPMe$_2$)(SiMe$_2$CH$_2$PMe$_2$)][N(SiMe$_2$CH$_2$PMe$_2$)$_2$] in $C_6D_5CD_3$ recorded at −29 °C (top) and a simulation (bottom) using Bruker PANIC software. See Table VI for details.

on the ancillary ligands, different variable-temperature NMR behavior is observed. For the complex YCl[N(SiMe$_2$CH$_2$PPh$_2$)$_2$]$_2$ (**1b**), the $^{31}P\{^1H\}$ NMR spectrum recorded at +29 °C shows the expected doublet ($^1J_{Y-P}$ = 39 Hz), indicating that all the phosphines are equivalent. However, at −59 °C the spectrum clearly shows four chemically inequivalent phosphorus-31 environments. This low-temperature-limiting spectrum has been simulated, and both the observed and calculated spectrum are shown in Figure 3. Three of the phosphines are coordinated to the metal, as shown by the $^1J_{Y-P}$ coupling constants, while the fourth appears to be dangling freely in solution (a sharp singlet that displays no coupling to either ^{89}Y or ^{31}P). The six-coordinate distorted octahedral geometry shown in Figure 3 is a possible structure for this complex. An analogous six-coordinate species could be one of the intermediates (undetected) for the fluxional process that exchanges all four phosphine sites in the chloro and hydrocarbyl complexes **1a**–**6a** containing −PMe$_2$ substituted ligands.

For the lanthanum complex with phenyls at phosphorus, LaCl[N(SiMe$_2$CH$_2$PPh$_2$)$_2$]$_2$ (**3b**), the $^{31}P\{^1H\}$ NMR spectrum is different again, as an apparent equilibrium between two species is observed. Above 80 °C, only one compound is present and it displays NMR spectra typical of the seven-coordinate fluxional species such as MCl[N(SiMe$_2$CH$_2$PR$_2$)$_2$]$_2$, R = Me, Ph. However, below −40 °C, a different complex is present, one that displays two uncoupled phosphorus environments which exchange with one another at high temperature. Between +80 and −40 °C both complexes are observable. It is possible that the complex seen at low temperature is a dimer which is in equilibrium with the monomer. That this proposed monomer/dimer behavior is not observed for yttrium and lutetium could be due to the smaller size of these metals relative to lanthanum, which because of its larger size could be capable of the eight-coordinate geometry that a chloride-bridged dimer would require. It is also possible that the complex LaCl[N(SiMe$_2$CH$_2$PMe$_2$)$_2$]$_2$ (**3a**) participates in such an equilibrium. However, at the crucial temperatures where differentiation between the two species might be observed, the $^{31}P\{^1H\}$ NMR spectra of this compound only show broad lines. Molecular weight determinations do show that the lanthanum complexes **3a** and **3b** are monomeric in C_6D_6 at 20 °C (at concentrations of 10–20 mg/mL).

The cyclometalated complexes derived from the loss of hydrocarbon (RH) from the yttrium or lutetium hydrocarbyl complexes MR[N(SiMe$_2$CH$_2$PMe$_2$)$_2$]$_2$ (eq 4) are also fluxional. At −29 °C for yttrium and +20 °C for lutetium, static $^{31}P\{^1H\}$ NMR spectra with four inequivalent phosphines are obtained; the low-temperature limit is not attained for the lanthanum derivative, **9a**, even down to −100 °C. At higher temperatures (T_c = −79 °C for lanthanum, +65 °C for yttrium, and +90 °C for lutetium, respectively) two of the phosphines exchange, while the metalated ligand remains rigid (ΔG^* = 8.8 kcal/mol for lanthanum (estimated), 15.3 kcal/mol for yttrium, and 16.3 kcal/mol for lutetium). The most consistent rationalization for this particular fluxional behavior is that the nonmetalated ligand has the phosphine arms rapidly dissociating and reassociating as already discussed for the chloro and hydrocarbyl derivatives. This enables these two phosphines to exchange coordination sites. The low-temperature-limiting spectra for the yttrium and lutetium complexes have been simulated as ABCD spin systems; the experimental and calculated spectra for the yttrium complex with methyls at phosphorus are shown in Figure 4 while the coupling constants for both are listed in Table VI.

The site of cyclometalation on the ligand backbone was determined by analysis of $^{13}C\{^1H\}$ NMR spectra for these complexes, since, in the low-temperature limit, only three methylene resonances (PCH$_2$Si) could be assigned while

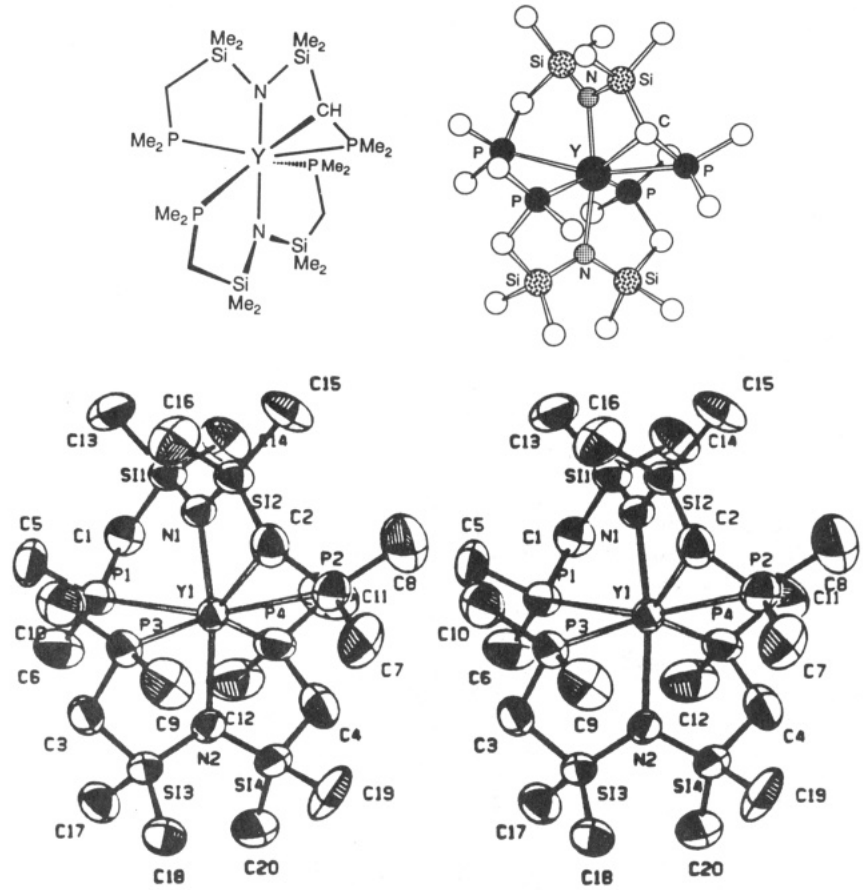

Figure 5. Molecular structure of **7a**: (bottom) an ORTEP stereoview showing the atom-labeling scheme and (top) a Chem 3D view showing the distorted capped octahedral environment at yttrium.

Table VI. $^2J_{P-P}$ and $^1J_{P-Y}$ Coupling Constants for M[N(SiMe$_2$CHPMe$_2$)(SiMe$_2$CH$_2$PMe$_2$)][N(SiMe$_2$CH$_2$PMe$_2$)$_2$]

coupling	M = Lu[a]	M = Y[b]
$^2J_{P1-P2}$	7.9	13.45
$^2J_{P1-P3}$	29.3	18.46
$^2J_{P1-P4}$	30.3	20.86
$^2J_{P2-P3}$	32.5	11.52
$^2J_{P2-P4}$	9.4	8.20
$^2J_{P3-P4}$	21.2	18.54
$^1J_{P1-Y}$		70.00
$^1J_{P2-Y}$		36.61
$^1J_{P3-Y}$		47.00
$^1J_{P4-Y}$		67.98

[a] At +20 °C: δ(P1) = −38.6 ppm, δ(P2) = −34.8 ppm, δ(P3) = −36.9 ppm, δ(P4) = −40.1 ppm. [b] At −29 °C: δ(P1) = −42.0 ppm, δ(P2) = −34.2 ppm, δ(P3) = −41.9 ppm, δ(P4) = −45.3 ppm.

all eight of the silyl methyls and phosphorus methyls were located; thus cyclometalation occurred at a methylene C–H.

X-ray Crystal Structure Determination of Y[N(SiMe$_2$CHPMe$_2$)(SiMe$_2$CH$_2$PMe$_2$)][N(SiMe$_2$CH$_2$PMe$_2$)$_2$]. The molecular structure is shown in Figure 5. This compound crystallizes in a capped octahedral geometry with the two nitrogens and the four phosphines forming a distorted octahedron with the metalated carbon as the capping ligand. The low-temperature $^{31}P\{^1H\}$ NMR spectrum is consistent with this structure; in fact the atom designations P1, P2, P3, and P4 in the crystal structure have been assigned in the $^{31}P\{^1H\}$ NMR spectrum (see caption for Table VI). P1 and P2 belong to the metalated ligand and are the nonfluxional phosphines. Since P2 is in a strained three-membered ring and therefore in the most different chemical environment, its assignment was made on the basis of the most unique chemical shift (−34.2 ppm). P2 also has the closest contact with the metal; therefore we would expect it to show the largest coordination contact shift. This then places P1 at −42.0 ppm. The assignment of the identity of the fluxional phosphorus atoms, P3 (at −41.9 ppm) and P4 (at 45.3 ppm), is purely arbitrary.

The four yttrium–phosphorus bond distances of 3.005 (3), 2.903 (3), 2.896 (3), and 2.817 (3) Å span a large bond length domain. There is only one other reported[5a] Y–P bond length to compare: Y(OCBu$^t_2$CH$_2$PMe$_2$)$_3$ has a Y–P bond length of 3.045 (2) Å. Presumably, the short Y–P2 bond length of 2.817 Å is due to the three-membered ring formed by the metalated carbon, yttrium, and P2. Other bond lengths for lanthanide–phosphine complexes range from 2.941 (3) Å for (η^5-C$_5$Me$_5$)$_2$YbCl(dmpm)[6d] to 3.154 (2) Å for Nd(OCBu$^t_2$CH$_2$PMe$_2$)$_3$.[5a]

The yttrium carbon bond length of 2.65 (1) Å is long for a yttrium–carbon σ bond. A typical bond length[23] is 2.47 Å, e.g. (η^5-C$_5$Me$_5$)$_2$YCH(SiMe$_3$)$_2$ has a Y–C bond length[24] of 2.468 (7) Å. Complexes that contain bridging alkyls have much longer Y–C bonds, e.g. [η^5-1,3-Me$_2$C$_5$H$_3$)$_2$Y(μ-Me)]$_2$ has Y–Me bond lengths[25] of 2.60 (1) and 2.62 (2) Å, and [(η^5-C$_5$H$_5$)$_2$Y(μ-Me)]$_2$ has a Y–Me bond length[26] of 2.655 (18) Å. The long Y–C interaction that we find in our complex could be due to the strain of the fused three- and

(23) Booij, M.; Kiers, N. H.; Meetsma, A.; Teuben, J. H.; Smeets, W. J. J.; Spek, A. L. *Organometallics* **1989**, *8*, 2454.
(24) den Haan, K. H.; de Boer, J. L.; Teuben, J. H.; Spek, A. L.; Kojic-Prodic, B.; Hays, G. R.; Huis, R. *Organometallics* **1986**, *5*, 2389.
(25) Evans, W. J.; Drummond, D. K.; Hanusa, T. P.; Doedens, R. J. *Organometallics* **1987**, *6*, 2279.
(26) Holton, J.; Lappert, M. F.; Ballard, D. G. H.; Pearce, R.; Atwood, J. L.; Hunter, W. E. *J. Chem. Soc., Dalton Trans.* **1979**, 54.

Table VII. Rate Data for the Thermolysis of $YR[N(SiMe_2CH_2PMe_2)_2]_2$

R = C_6H_5		R = $CH_2C_6H_5$		R = $CD_2C_6D_5$		$k_{obs}(CH_2C_6H_5)/k_{obs}(CD_2C_6CD_5)$
temp, °C	k_{obs}	temp, °C	k_{obs}	temp, °C	k_{obs}	
		43.0	8.03×10^{-3}			
47.0	8.25×10^{-2}	47.0	1.08×10^{-2}	47.0	1.23×10^{-2}	0.88
		50.0	1.43×10^{-2}			
56.6	2.43×10^{-2}	56.5	2.97×10^{-2}	56.5	3.36×10^{-2}	0.88
60.0	3.25×10^{-2}					
66.0	5.86×10^{-2}	66.5	7.19×10^{-2}	66.5	8.49×10^{-2}	0.85
73.0	9.91×10^{-2}	73.5	1.42×10^{-1}	73.5	1.55×10^{-2}	0.92
		75.5	1.83×10^{-1}	75.5	2.02×10^{-1}	0.91

Table VIII. Eyring Data for the Thermolysis of $YR[N(SiMe_2CH_2PMe_2)_2]_2$

function	R = C_6H_5	R = $CH_2C_6H_5$	R = $CD_2C_6D_5$
correlation	−0.998	−0.999	−0.999
$\Delta S^{\ddagger}$, cal/K/mol	−4.1 ± 3	−3.3 ± 3	−2.7 ± 3
$\Delta H^{\ddagger}$, kcal/mol	20.5 ± 1	20.6 ± 1	20.7 ± 1

four-membered Y–C2–P2 and Y–C2–Si2–N1 rings.

Kinetics of the Thermolysis of $MR[N(SiMe_2CH_2PMe_2)_2]_2$. As already mentioned, the yttrium and lutetium hydrocarbyl complexes **4a–6a** eliminate hydrocarbon upon mild thermolysis by abstraction of a PCH_2Si–methylene hydrogen to generate the cyclometalated complexes shown in eq 4. The transformation can be conveniently followed by $^{31}P\{^1H\}$ NMR spectroscopy by measuring the decrease in concentration of the starting hydrocarbyl complex; this reaction shows clean first-order kinetics over a wide temperature range, as shown by the results in Table VII and in Figure 6 for the yttrium–phenyl and –benzyl complexes, **4a** and **5a**. From the Eyring plots, the activation parameters (Table VIII) are remarkably similar: $\Delta H^{\ddagger} = 20.5$ (1) kcal/mol and $\Delta S^{\ddagger} = -3$ (3) eu. The standard four-centered transition state[27] normally invoked for this type of process is generally associated with a large, negative $\Delta S^{\ddagger}$. To account for the rather small, but negative $\Delta S^{\ddagger}$'s observed in this work, a transition state with a dissociated phosphine would be expected to have additional degrees of freedom and to be better able to align into the necessary four-centered configuration for hydrocarbon elimination; such a possibility is shown in II.

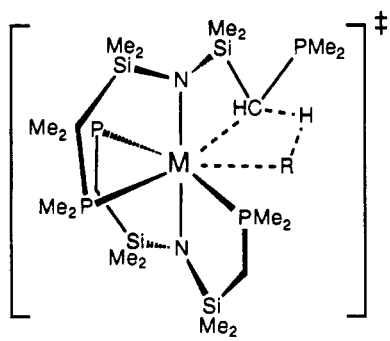

II

Another interesting feature of this reaction is an *apparent* inverse isotope effect exhibited by the decomposition of $YR[N(SiMe_2CH_2PMe_2)_2]_2$, R = $CH_2C_6H_5$, $CD_2C_6D_5$. Even though the only C–H bonds being broken and formed in the transition state involve a PCH_2Si–methylene hydrogen being transferred to the benzyl ligand to form toluene ($CH_3C_6H_5$ and $CHD_2C_6D_5$), the formation of $CHD_2C_6D_5$ is faster than the formation of $CH_3C_6H_5$: $k_H/k_D = 0.85$–0.92 in the temperature range studied. One way to explain this observation is to invoke[28] a preequilibrium involving an agostic η^2-benzyl ligand going to η^1-benzyl

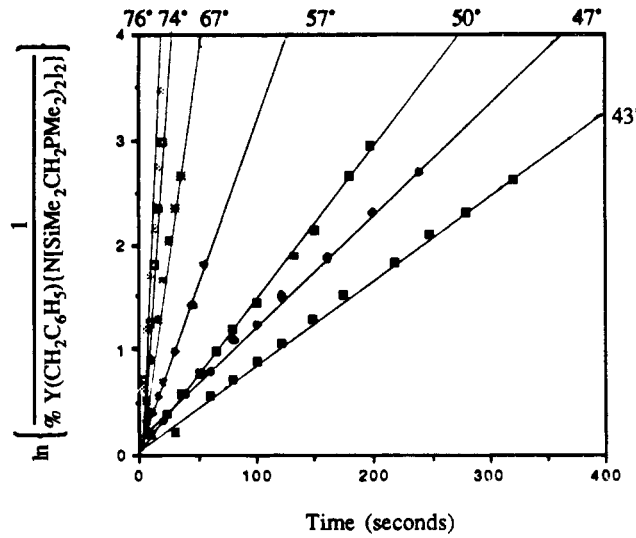

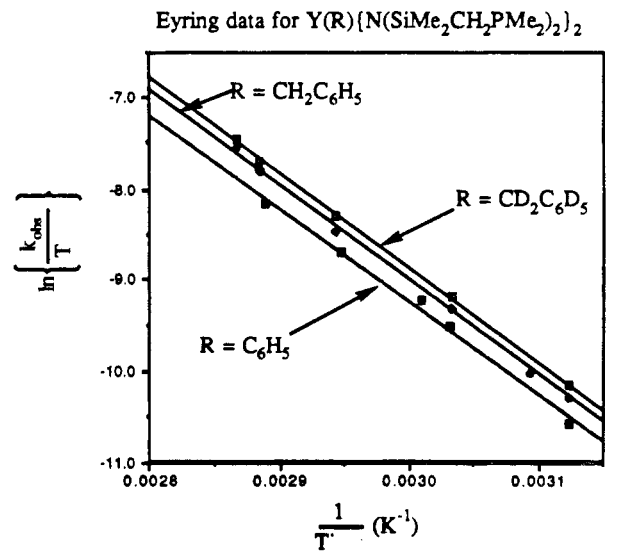

Figure 6. (a, top) First-order rate plots for the thermolysis of $Y(CH_2C_6H_5)[N(SiMe_2CH_2PMe_2)_2]_2$. (b, bottom) Eyring plots for the thermolysis of $Y(R)[N(SiMe_2CH_2PMe_2)_2]_2$, where R = $CH_2C_6H_5$, $CD_2C_6D_5$, and C_6H_5.

Scheme I

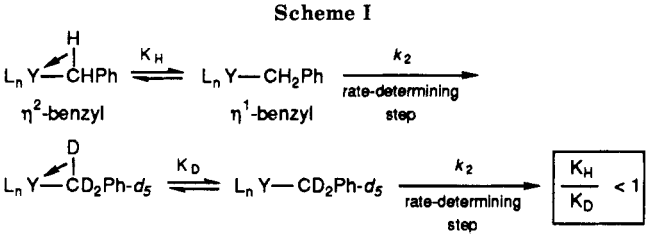

prior to the loss of toluene (Scheme I). For these molecules, the breaking of an agostic benzyl C–H→Y (or C–D→Y) interaction could be required in order for the benzyl ligand to achieve the required geometry for the elimination

(27) Rothwell, I. P. *Polyhedron* **1985**, *4*, 177.
(28) Parkin, G.; Bercaw, J. E. *Organometallics* **1989**, *8*, 1172.

sequence. Since an agostic C–H→M is a stronger interaction then C–D→M, any preequilibrium would generate a higher concentration of η^1-$CD_2C_6D_5$ than η^1-$CH_2C_6H_5$, resulting in faster elimination of $CHD_2C_6D_5$ than $CH_3C_6H_5$. The measured deuterium isotope effect is therefore determined by the thermodynamic equilibrium isotope effect of the preequilibrium ($K_H/K_D < 1$), as the kinetic deuterium isotope effect should be near unity. In addition, the increase in k_H/k_D from 0.85 to 0.92 as the temperature increases is consistent with $k_{obs} = K_{eq}k_2$ (where K_{eq} refers to the preequilibrium and k_2 corresponds to the rate-determining step).

Unfortunately, there is no conclusive evidence for the assumed agostic benzyl ligand. These compounds do display a reduced $^1J_{C-H}$ coupling of 115 Hz, a typical agostic spectroscopic feature. However, no evidence for an agostic C–H was evident in the solid-state IR spectra. We had hoped that the activation parameters for this reaction sequence would provide further evidence for this preequilibrium of the agostic benzyl ligand. Unfortunately, because the difference between the rates k_H and k_D is so small, the calculated activation parameters are, within experimental error, indistinguishable: $\Delta H^{\ddagger}_{d_0}$ = 20.6 kcal/mol, $\Delta H^{\ddagger}_{d_7}$ = 20.7 kcal/mol, $\Delta S^{\ddagger}_{d_0}$ = −3.3 eu, $\Delta S^{\ddagger}_{d_7}$ = −2.7 eu. The activation parameters for the thermolysis of the phenyl complex are similar: $\Delta H^{\ddagger}$ = 20.5 kcal/mol, $\Delta S^{\ddagger}$ = −4.1 eu.

It is interesting to compare the rates of cyclometalation for the various $MR[N(SiMe_2CH_2PMe_2)_2]_2$ complexes as a function of M and R. At 73 °C, the lutetium–phenyl complex ($k = 1.88 \times 10^{-4}$ s^{-1}, half-life ($\tau_{1/2}$) = 61.3 min) is 1 order of magnitude more stable than the corresponding yttrium–phenyl complex ($k = 1.65 \times 10^{-3}$ s^{-1}, $\tau_{1/2}$ = 7.0 min), which in turn is more stable than the yttrium–benzyl complex ($k = 2.37 \times 10^{-3}$ s^{-1}, $\tau_{1/2}$ = 4.9 min). The difference between the two yttrium complexes is rather small and may reflect the stronger Y–C_{sp^2} bond of the phenyl derivative as compared to the Y–C_{sp^3} bond of the benzyl complex. The difference in rates between Lu and Y is probably due to the smaller size of lutetium relative to yttrium, thus making it more difficult for the lutetium derivative to attain the strained four-centered transition state. Consistent with this is the fact that the lanthanum–phenyl complex was not isolable; since the La^{+3} ion is the largest, the activation barrier is lowered.

Reactivity of $M[N(SiMe_2CHPMe_2)(SiMe_2CH_2PMe_2)][N(SiMe_2CH_2PMe_2)_2]$ (M = Y, Lu). The strained structure depicted by the X-ray crystal structure determination prompted us to see if this complex might undergo σ-bond metathesis[29] reactions. Indeed, in a sealed NMR tube under approximately 4 atm of D_2, the M–C bond does react reversibly, presumably generating the undetectable (by NMR spectroscopy) deuteride $YD[N(SiMe_2CHDPMe_2)(SiMe_2CH_2PMe_2)][N(SiMe_2CH_2PMe_2)_2]$, which can then eliminate HD by a further ligand cyclometalation reaction (Scheme II). However, this reaction only proceeds at high temperatures. No reaction was detected until the NMR tube had been heated to about 90 °C for several hours. At this point, HD (triplet at 4.42 ppm, $^1J_{H-D}$ = 42.6 Hz) and H_2 (at 4.46 ppm) were detectable. When deuterium NMR spectra were run on these complexes it was found that all the $Si(CH_3)_2$ and $SiCH_2P$ positions but *not* the $P(CH_3)_2$ protons in the amido–diphosphine ligand had been deuterated. Clearly,

Scheme II

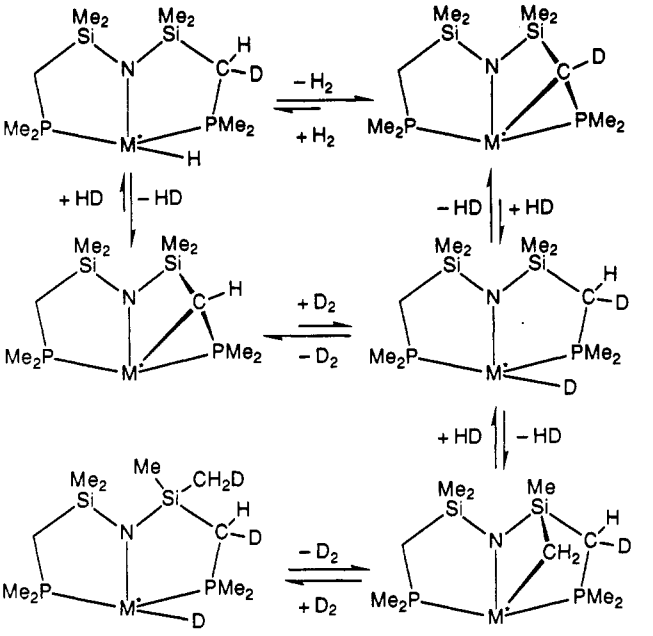

M = M[N(SiMe2CH2PMe2)2]

it must be possible to metalate at both of these positions from the ligand to the metal, but the thermodynamic product is with metalation at the methylene position. A possible mechanism for this process is shown in Scheme II.

Unfortunately, these complexes will only activate their own C–H bonds. When a toluene-d_8 solution of the yttrium complex was placed under H_2 and heated to 110 °C for 1 week, no HD was detectable in the NMR spectrum. If any of the toluene-d_8 were activated by this complex, then eventually the deuterium label would appear in the H_2 gas. In addition, a deuterium NMR spectrum was obtained that showed no deuterium incorporation in the complex. The same results were obtained from sealed samples of both complexes in just toluene-d_8. After extensive heating, ^{2}H NMR spectra showed no uptake of deuterium into the complexes. Also, a cyclopentane-d_0 solution of the yttrium complex was placed under approximately 4 atm of D_2 and heated to 95 °C for 1 week. Mass spectral analysis of the cyclopentane showed no increase above natural-abundance deuterium. Thus, although these cyclometalated compounds are thermally robust (no decomposition of these complexes has been detected even when heated to 110 °C for 1 week) and will engage in σ-bond metathesis with H_2 and D_2, they appear to be too sterically crowded to react with larger molecules.

Conclusions

The strategy to use a hybrid ligand containing an amide donor flanked by two phosphine groups has allowed for the preparation of a series of complexes of the group 3 elements Y and La and the lanthanide metal Lu that contain phosphine donors. These bis(ligand) complexes of the general formula $MCl[N(SiMe_2CH_2PR_2)_2]_2$ are seven-coordinate and formally isoelectronic to the bis(cyclopentadienyl) derivatives $(\eta^5\text{-Cp}')_2MCl$ (Cp′ = C_5H_5, C_5Me_5). However, these cyclopentadienyl derivatives have the "bent" metallocene structure and therefore have completely different geometries than that observed for these phosphine complexes. One result of this structural difference is that the metallocene derivatives form adducts

(29) Thompson, M. E.; Baxter, S. M.; Bulls, A. R.; Burger, B. J.; Nolan, M. C.; Santarsiero, B. D.; Schaefer, W. P.; Bercaw, J. E. *J. Am. Chem. Soc.* **1987**, *109*, 203.

with THF, LiCl, and KCl and exist as dimers in the absence of such ligands.[30] In contrast, no such adducts form with the bis(amido–diphosphine) complexes MCl[N-($SiMe_2CH_2PR_2$)$_2$]$_2$, thus indicating that these phosphine complexes are quite sterically saturated.

Both the starting chloro complexes MCl[N-($SiMe_2CH_2PR_2$)$_2$]$_2$ and the corresponding hydrocarbyl derivatives MR[N($SiMe_2CH_2PMe_2$)$_2$]$_2$ are found to be fluxional by NMR spectroscopy. For those complexes having methyl substituents at phosphorus (**a** series), a pentagonal–bipyramidal structure in the low-temperature limit is consistent with the spectroscopic data, particularly the $^{31}P\{^1H\}$ NMR spectra. The nature of the fluxional process that exchanges all of the phosphorus-31 sites is proposed to be phosphine-arm dissociation followed by rearrangement and reassociation. Other studies, namely the kinetics of cyclometalation and the low-temperature behavior of the diphenylphosphine derivatives (**b** series), that show one phosphine arm dangling from an octahedral geometry, are in agreement with this proposal.

Hydrocarbyl derivatives of the early-transition-metal elements and the lanthanides have been shown to be especially prone to olefin insertion and as a result are often used as catalysts or as models for catalysts in Ziegler–Natta polymerization studies.[31] The yttrium and lutetium bis(ligand) hydrocarbyl derivatives, MR[N-($SiMe_2CH_2PMe_2$)$_2$]$_2$, are thermally sensitive and undergo hydrocarbon elimination to form the cyclometalated derivatives M[N($SiMe_2CHPMe_2$)($SiMe_2CH_2PMe_2$)][N-($SiMe_2CH_2PMe_2$)$_2$]. The analogous cyclometalated lanthanum derivative is isolated directly upon metathesis of the chloro starting complex. Any attempts to examine hydrogenolysis or insertion reactions of these particular hydrocarbyl derivatives have resulted in the formation of these very stable products in which one of the ligands has been metalated; this has so far hampered all attempts to probe the effect of phosphine ancillary ligands on the reactivity patterns of early metal–hydrocarbyl moieties.

The mechanism of the cyclometalation process has a number of notable features. Firstly, the very small, but negative ΔS^* measured can be accounted for by invoking phosphine dissociation prior to the formation of the highly ordered four-centered transition state; this provides additional degrees of freedom for the transition state and allows easier alignment of the hydrocarbyl and carbon–hydrogen groups for elimination. Secondly, the secondary inverse isotope for the elimination of toluene from Y(CH_2Ph)[N($SiMe_2CH_2PMe_2$)$_2$]$_2$ versus the elimination of toluene-d_7 from Y(CD_2Ph-d_5)[N($SiMe_2CH_2PMe_2$)$_2$]$_2$ is consistent with an agostic interaction of the α-hydrogens of the benzyl ligands; thus a preequilibrium of the η^2-benzyl to an η^1-benzyl is necessary before the four-centered transition state is formed. Lastly, the effect of the metal on the rate of the cyclometalation process is rather pronounced. The increase in rate as one goes from Lu to Y to La perfectly mirrors the increase in the ionic radii of the M(III) centers and suggests that because the transition state is seven-coordinate, its formation occurs more readily for larger metal ions.

One of the most important results of this study is that the particular ancillary ligand design has illustrated for the first time the use of phosphorus NMR spectroscopy as a tool to assign the stereochemistry of early metal and lanthanide complexes. Not only can one observe the fluxional process but also analysis of low-temperature-limiting spectra gives insights into probable geometries.

Although we cannot as yet gauge the strength of the early-metal-to-phosphine interaction, the fact that ligand dissociation is facile suggests that this interaction is weak. It should be noted however that our design of ligands that incorporate the phosphine donor into a chelate array overcomes this thermodynamic instability and provides for kinetically stable phosphine complexes of the early metals and the lanthanides.

Acknowledgment. We gratefully acknowledge NSERC of Canada for financial support in the form of operating grants and an E. W. R. Steacie Fellowship to M.D.F. Acknowledgment is also made to the donors of the Petroleum Research Fund, administered by the American Chemical Society, for partial support of this work.

Supplementary Material Available: An ORTEP diagram with hydrogen atoms included and tables of hydrogen atom parameters, anisotropic thermal parameters, torsion angles, intermolecular contacts, and least-squares planes (12 pages); a listing of measured and calculated structure factor amplitudes (51 pages). Ordering information is given on any current masthead page.

(30) Evans, W. J.; Peterson, T. T.; Rausch, M. D.; Hunter, W. E.; Zhang, H.; Atwood, J. L. *Organometallics* **1985**, *4*, 554.

(31) (a) Watson, P. L.; Parshall, G. W. *Acc. Chem. Res.* **1985**, *18*, 51. (b) Jeske, G.; Lauke, H.; Mauermann, H.; Swepston, P. N.; Schumann, H.; Marks, T. J. *J. Am. Chem. Soc.* **1985**, *107*, 8091. (c) Bunel, E.; Burger, B. J.; Bercaw, J. E. *J. Am. Chem. Soc.* **1988**, *110*, 976.